DOI: https://doi.org/10.36094/sc.v89.2025.Multi_Scale_Recurrence_Quantification_Analysis.Sharma_Naidu.73

ARTICLE

Sci. and Cult. 91 (1–2) : 73-82 (2025)

MULTI-SCALE RECURRENCE QUANTIFICATION ANALYSIS OF TIME SERIES FOR BEARING HEALTH MONITORING

ANJU SHARMA[1] AND V.P.S. NAIDU[2*]

Integrated Vehicle Health Management (IVHM) systems play a crucial role in ensuring the safety, reliability, and efficiency of modern aircraft by monitoring critical components such as bearings, which are integral to engines, landing gear, and control surfaces. This study presents a novel method combining Discrete Wavelet Transform (DWT) and Recurrence Plots for bearing health monitoring. DWT is used to decompose signals into frequency bands via high-pass and low-pass filters, and the resulting signals are analyzed with Recurrence Quantification Analysis (RQA) to extract 91 features. These features are utilized for fault classification using C-Support Vector Machine (CSVM), Quadratic Support Vector Machine (QSVM), and Linear Discriminant Analysis (LDA). Initially, employing all 91 features resulted in perfect training accuracy (100%) across all classifiers. Feature selection using error plots identified two optimal features, yielding training accuracies between 82.7% and 84.3% and testing accuracies from 80.2% to 86.4%. Further analysis demonstrated that the QSVM achieved the highest testing accuracy among the selected features, while the CSVM consistently delivered 100% testing accuracy. With feature selection algorithms, LDA achieved a training accuracy of 98.4% and a testing accuracy of 98.8%, whereas QSVM and Cubic SVM both attained 99.7% training accuracy, with QSVM reaching 98.8% testing accuracy and Cubic SVM achieving perfect 100% testing accuracy. These results highlight the effectiveness of integrating wavelet-based feature extraction with advanced classification techniques for accurate and efficient bearing fault diagnosis, significantly enhancing predictive maintenance practices.

Keywords: *Condition monitoring, Multi-scale recurrence quantification analysis, machine learning, fault classification, bearing health monitoring.*

Introduction

Integrated Vehicle Health Management (IVHM) systems have become indispensable for the aviation industry, ensuring the continuous monitoring and maintenance of aircraft systems to uphold safety, reliability, and efficiency standards. Among the myriad components that contribute to aircraft functionality, bearings are of paramount importance, as they support critical systems such as engines, landing gear, and control surfaces. Consequently, the health of these bearings directly impacts the overall performance and safety of the aircraft. In light of this, bearing health monitoring has emerged as a pivotal aspect of IVHM, aiming to detect potential faults or degradation in bearings at an early stage. Early detection is crucial to pre-emptively address issues and prevent catastrophic failures, which could compromise the safety

1 CSIR-National Aerospace Laboratories, Bengaluru 560017, India

2 Academy of Scientific and Innovative Research, Ghaziabad 201002, India

* Corresponding Author: vpsnaidu@nal.res.in

and operational integrity of the aircraft. The need for the condition monitoring of machines could be understood by the following accidents which occurred due to bearing failure.

- Between 2007 and 2008, there were 12 occurrences of the bearing failures of wheels on express freight wagons, leading to derailments. Fig. 1 shows the derailed wagon and the failed wheel bearing, a notable case was the 2007 Huntly derailment, where a failed wheel bearing on the third wagon caused the derailment of nine additional wagons, scattering debris over 4 kilometres[1]

Fig. 1: Freight wagons derailment- Huntly[1]

- On June 10, 2014, a Boeing 737 at Sydney Airport experienced shuddering while taxiing. Investigation revealed a fatigue-induced crack in the landing gear, leading to its failure [2]. Fig. 2 depicts some of the broken parts of the aircraft.

Similarly, several other incidents have occurred due to the failure or bearings or any other parts of an air vehicle. Advanced techniques and methodologies are constantly being developed and incorporated into IVHM systems to enhance monitoring capabilities. One such technique for monitoring bearing conditions is the use of recurrence plots. These plots visually depict the recurring patterns within a signal, providing valuable insights into the dynamic behavior and regularities in the data. Recurrence plots are then analyzed using Recurrence Quantification Analysis (RQA), which is used to quantify the properties of these plots to extract meaningful features that indicate the bearing's health status.

Fig. 2: Boeing 737 Sydney aircraft accident[2]

Ref[3] provides insights into fault detection within a rotary system and the identification of bearing operational parameters through the analysis of nonlinear dynamics. In Refs[4-5], a fault classification approach is introduced, leveraging vibration signals from bearings and employing recurrence-plot analysis along with a Convolutional Neural Network (CNN) for image-based fault diagnosis. Ref[6] is a study that utilizes recurrence plots (RP) to transform data, like 3-phase signals which are from current sensors, into 2D texture images, which are then processed by a convolutional neural network (CNN) to extract robust features for diagnosing fault conditions in induction motors by classifying these images, with testing conducted on a dataset from various 3-phase motors exhibiting different failure modes. Ref[7] explores the impact of noise on recurrence plots and quantifiers through the analysis of denoised vibration data. Ref [8] demonstrates the

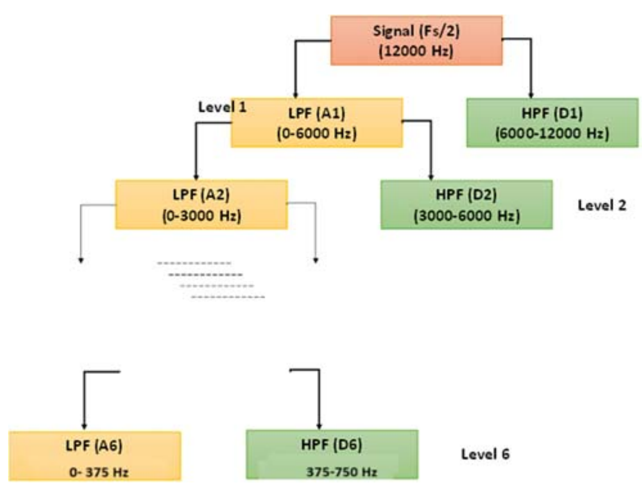

Fig. 3: Decomposition steps using DWT

classification of electric motor problems using stator-current measurements and recurrence quantification analysis (RQA). The use of recurrence plots and recurrence quantification analysis for identifying a range of faults is showcased[9]. Ref[10] introduces a unique framework for problem diagnosis, highlighting the efficacy of recurrence quantification analysis (RQA) in handling noisy signals. A strategy for feature development from raw vibration data for bearing defect classification, based on RQA, is presented in Ref[11], demonstrating improved performance compared to conventional approaches. Lastly, for the evaluation of bearing degradation, Ref[12] proposes an integrated strategy that combines RQA with the Kalman filter. This article suggests using machine learning methods such as linear discriminant analysis and Support Vector Machines (SVMs) for recurrence quantification analysis in detecting bearing failures. Ref[13,14] studies the different trends and novel directions of using recurrence plots with machine learning algorithms.

The novelty of this study lies in its integration of advanced signal processing and feature selection techniques for fault diagnosis in motor bearings. Specifically, the use of Discrete Wavelet Transform (DWT) to extract a comprehensive set of features, followed by rigorous feature selection methods to identify the utmost significant features, represents a sophisticated approach to optimizing diagnostic accuracy. The study also showcases the effectiveness of combining traditional classifiers with these optimized features, demonstrating that even with a reduced feature set, high classification accuracy can be maintained, particularly with the Quadratic and Cubic Support Vector Machines (SVMs). The achievement of perfect testing accuracy with the Cubic SVM highlights the potential of this method for highly reliable fault detection in practical applications. This methodological innovation offers a significant contribution to the field of predictive maintenance and fault diagnosis.

Recurrence Plots

Recurrence Plots (RP) visually represent the recurrence of patterns in time series data, developed by Eckmann et al. in 1987. They plot the distances between data points against time, highlighting recurring patterns as diagonal lines. RP aids in exploring complex system dynamics, especially chaotic or nonlinear behaviours. Alongside Recurrence Quantification Analysis (RQA), RP allows for the extraction of features like determinism (DET), entropy (ENT), and the length of the longest diagonal (L). This combined approach provides insights into hidden patterns and transitions within the data, facilitating a deeper understanding of complex system behaviours. In this work, 13 features have been extracted from the RP when the embedded dimension (m) is 1 and threshold (th) is 0.1. The list of the features and their significance are listed in

Table 1 Features from Recurrence Plots

Feature No.	Feature Name	Significance
F1	Recurrence Rate (RR)	Indicates the frequency of recurrent patterns, reflecting system stability.
F2	Determinism (DET)	Measures predictability, with higher values suggesting regular dynamics.
F3	Laminarity (LAM)	Quantifies pattern persistence, revealing system regularity.
F4	Average Diagonal Line Length (L)	Reflects the duration of recurrent patterns and system persistence.
F5	Trapping Time (TT)	Indicates average time trajectories remain trapped within patterns, revealing stability.
F6	Maximum Diagonal Length, L_{max}	Highlights presence of long-term recurrent patterns and system stability.
F7	Divergence (DIV)	Measures trajectory divergence/convergence, indicating dynamic behaviour.
F8	Shannon Entropy (ENTR)	Quantifies complexity and uncertainty, reflecting system irregularity.
F9	Trend	Reveals directional trends and asymmetries in system dynamics.
F10	Ratio	Refers to a specific metric or calculation comparing different aspects of the recurrence plot, such as the ratio of vertical to horizontal lines or the ratio of certain features within the plot.
F11	Recurrence Period Density Entropy (RPDE)	Measures irregularity and complexity in recurrence periods.
F12	Clustering Coefficient	Indicates connectivity among recurrent points, revealing network structure.
F13	Transitivity	Reflects the presence of interconnected and coherent patterns in the data.

Table 1. Each feature alone may not be able to represent the fault completely, but a combination of these features will definitely be helpful in finding the faults easily.

Discrete Wavelet Transform (DWT)

Discrete Wavelet Transform (DWT) is a powerful mathematical tool used for signal processing, particularly in the analysis of time-series data. It decomposes a signal into different frequency components, known as wavelets, allowing for a multi-resolution analysis. In the DWT process, the signal is made to pass through a sequence of high-pass and low-pass filters, charted by down-sampling, resulting in detailed coefficients representing high-frequency components and an approximate coefficient representing the low-frequency component. In this work, the coefficients are found up to 6 levels, as shown in Fig. 3. After level 6, there was no significant data on which features could be derived. 13 features are extracted from each level along with features from the last approximate coefficient, i.e., from each level, the 13 features of Table 1 have been extracted. This makes for 13x7=91 features in total.

Methodology

This study utilizes the bearing dataset sourced from Case Western Reserve University, focusing on motor bearings intentionally seeded with defects. These defects vary in diameter from 0.007 inches to 0.04 inches. Vibration data from these bearings is recorded using accelerometers mounted on the bearing housing. Specifically, we analyze the drive end dataset, which was sampled at a rate of 12000 samples per second. The dataset comprises four distinct categories of data: data from three different defects (ball defect, inner race defect, and outer race defect), along with normal data. All the defect data are decomposed using DWT and features are obtained from the time series data utilizing multi-scale recurrence quantification analysis. The proposed methodology is shown in Fig. 4. The following points show the significance of features linked with bearing fault conditions (Normal, Ball defect, Inner race defect, Outer race defect).

Normal Condition: Features extracted from signals under normal conditions typically show consistent, predictable patterns with minimal variation. Features related to normal conditions generally have stable values with little noise.

Ball Defect: Ball defects often cause periodic impacts and irregular vibrations. Features linked to ball defects may include increased periodicity or higher amplitude in the frequency domain, reflecting the repetitive nature of the defect.

Inner Race Defect: An inner race defect usually results in vibration patterns with specific fault frequencies. Features related to inner race defects may show increased amplitudes at these characteristic frequencies or specific patterns indicative of localized defects.

Outer Race Defect: Outer race defects can cause vibrations at certain fault frequencies that differ from those of inner race defects. Features associated with outer race defects may show prominent peaks at these frequencies or distinct changes in vibration patterns.

Results and Discussion

In this study, as previously mentioned, 91 features are extracted from the coefficients obtained through the Discrete Wavelet Transform (DWT). The mean ± standard deviation of these 91 features is tabulated in Table 2. Data classification was performed by employing three approaches: First, using all 91 features simultaneously; Second, utilizing only the best non-overlapping features obtained from error plots; and Third, by selecting the best features through different feature selection algorithms. The results of these classification approaches are elaborated below. Data classification was carried out using C-Support Vector Machine (CSVM), Quadratic Support Vector Machine (QSVM), and Linear Discriminant Analysis (LDA) algorithms.

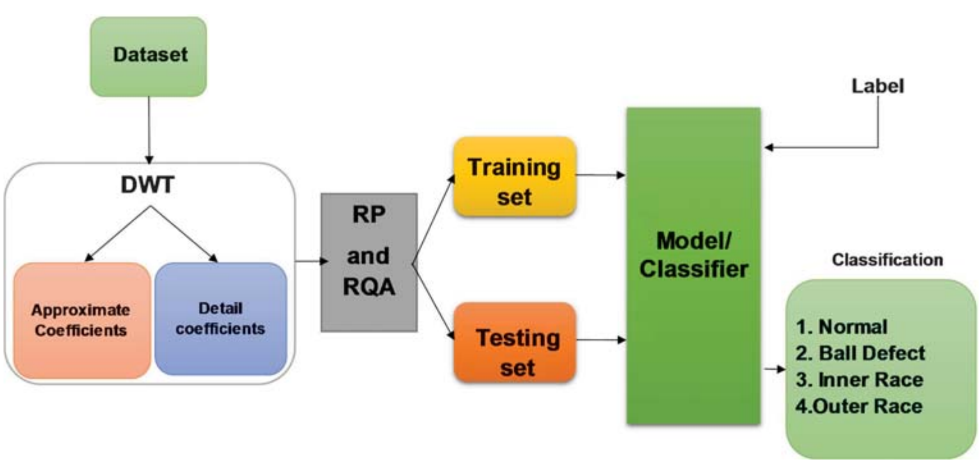

Fig. 4: Proposed Methodology

Table 2 Mean ± standard deviation of the features extracted

Mean ± Standard deviation				
Feature	**Normal**	**Ball defect**	**Inner race defect**	**Outer race defect**
Fm1	0.992814461 ±0.0028865	0.202117233 ±0.0598464	0.057541514 ±0.0118017	0.082889288 ±0.0412442
Fm2	0.999859769 ±0.000141	0.798533088 ±0.0459003	0.530340951 ±0.1380914	0.587867518 ±0.1141844
Fm3	154.3066719 ±58.747658	3.870072566 ±0.3328371	2.852763927 ±0.2695343	2.961583861 ±0.4230371
Fm4	4088.407767 ±1.8970421	52.33035714 ±8.342217	34.86725664 ±8.4773905	32.00892857 ±7.8871495
Fm5	0.406270868 ±0.0307515	0.18958833 ±0.0220378	0.115153948 ±0.0313857	0.126550961 ±0.0283063
Fm6	0.999943346 ±4.71E-05	0.30366723 ±0.1081203	0.195841999 ±0.0276119	0.311808026 ±0.1524401
Fm7	156.1212928 ±60.399872	3.389972434 ±0.1963891	2.820418617 ±0.4622414	3.03779194 ±0.4401776
Fm8	4090.466019 ±3.5608043	38.78571429 ±12.213881	20.38938053 ±7.8027395	24.94642857 ±12.184645
Fm9	3.432038835 ±1.4559358	2049.205357 ±622.2228	3422.548673 ±315.28284	3754.589286 ±180.84459
Fm10	1.038960326 ±0.0458945	5.397751605 ±1.4551304	18.36049059 ±4.1122169	15.38550294 ±6.3064456
Fm11	0.017729789 ±0.0147988	0.260121019 ±0.0325328	0.408099016 ±0.0133077	0.362619652 ±0.0588139
Fm12	0.993572554 ±0.0024876	0.656225861 ±0.0253317	0.595952693 ±0.0035392	0.6186274 ±0.0224816
Fm13	0.993301077 ±0.0025046	0.634713327 ±0.0264413	0.602282504 ±0.0071872	0.633284801 ±0.0359618
Fm14	0.638590952 ±0.0308063	0.124045834 ±0.0372165	0.027017312 ±0.0108521	0.044200681 ±0.024132
Fm15	0.823890092 ±0.0269933	0.438213355 ±0.0795623	0.153405651 ±0.0450386	0.272678162 ±0.0701297
Fm16	5.705974785 ±0.2291119	2.466968493 ±0.1492107	2.162694082 ±0.0776777	2.282280189 ±0.0838877
Fm17	637.9563107 ±227.44507	18.82142857 ±4.2367212	10.99115044 ±3.01335	12.71428571 ±3.1720303
Fm18	0.208469843 ±0.0128771	0.099311544 ±0.017391	0.039934876 ±0.0099468	0.064907565 ±0.0142832
Fm19	0.876447103 ±0.0212806	0.550267786 ±0.0940427	0.243674708 ±0.0746893	0.407283994 ±0.0868729
Fm20	3.628102846 ±0.3614607	2.545114534 ±0.1780154	2.227420343 ±0.1229699	2.435351796 ±0.1655834
Fm21	79.41747573 ±11.042732	15.3125 ±4.9792927	7.380530973 ±2.5680683	11.41071429 ±3.8263043
Fm22	99.5631068 ±122.08199	1284.401786 ±290.31531	1786.840708 ±123.99068	1831.883929 ±108.99374
Fm23	1.548024724 ±0.0545478	11.29910982 ±3.0169116	42.11615298 ±17.485103	30.81181946 ±15.138044
Fm24	0.121430079 ±0.0066611	0.424795644 ±0.0421618	0.583858808 ±0.0551913	0.522708994 ±0.0710123
Fm25	0.82983892 ±0.0118989	0.619656543 ±0.0162326	0.578398267 ±0.0083018	0.594308924 ±0.0149818
Fm26	0.809674076 ±0.0154903	0.602410598 ±0.016234	0.574424365 ±0.0068942	0.596006087 ±0.0251941
Fm27	0.332132853 ±0.0523888	0.427367338 ±0.1281926	0.085984929 ±0.0394035	0.11143708 ±0.0300996
Fm28	0.582356927 ±0.0572654	0.658032652 ±0.1533594	0.19498954 ±0.0869145	0.30161965 ±0.0563264
Fm29	2.97898242 ±0.0946478	2.942521042 ±0.397422	2.172344876 ±0.0828682	2.27169796 ±0.074814
Fm30	37.5776699 ±7.598542	42.25892857 ±11.231989	12.71681416 ±6.4302147	12.39285714 ±3.6744973
Fm31	0.146217638 ±0.0143717	0.165248824 ±0.0430874	0.052964184 ±0.0200006	0.077514711 ±00128547
Fm32	0.571759993 ±0.0802704	0.692474649 ±0.1141001	0.227041203 ±0.0605673	0.314259438 ±0.0451296
Fm33	2.682014579 ±0.1810886	3.263418825 ±0.4654734	2.226046654 ±0.138048	2.37616171 ±0.0986669
Fm34	25.50485437 ±6.0717238	32.51785714 ±18.21443	7.309734513 ±3.4358396	10.28571429 ±2.7977744
Fm35	371.3834951 ±141.52309	282.8839286 ±156.11862	742.1858407 ±108.52424	778.2946429 ±117.23901
Fm36	3.216086001 ±0.6388786	2.935306244 ±1.3406045	13.85533879 ±5.6558076	9.565328339 ±2.4086625
Fm37	0.267227123 ±0.0238068	0.238573186 ±0.0599672	0.48483154 ±0.0678415	0.430259426 ±0.0344071
Fm38	0.703997414 ±0.0162554	0.735327753 ±0.0482905	0.605454219 ±0.0162895	0.618514084 ±0.0120522
Fm39	0.67720811 ±0.0179403	0.707051063 ±0.0525256	0.591268659 ±0.0185188	0.613779044 ±0.0110685

Feature	Normal	Ball defect	Inner race defect	Outer race defect
Fm40	0.314276739 ±0.0345576	0.316065185 ±0.027696	0.053349924 ±0.0127721	0.053835724 ±0.0211915
Fm41	0.540596796 ±0.0431961	0.530785355 ±0.0418813	0.115480012 ±0.023663	0.124336495 ±0.0298539
Fm42	2.491673585 ±0.0693097	2.475329043 ±0.0734358	2.081159271 ±0.0252351	2.084180472 ±0.0318846
Fm43	18.05825243 ±3.1478223	18.14285714 ±3.2793571	5.610619469 ±1.5378187	5.6875 ±1.7503217
Fm44	0.144218433 ±0.0112889	0.141668334 ±0.0111547	0.038326842 ±0.0065698	0.040629098 ±0.0079455
Fm45	0.581728045 ±0.0697261	0.572404731 ±0.0378224	0.145957694 ±0.0343585	0.179492935 ±0.0489759
Fm46	2.718625141 ±0.1396597	2.677375634 ±0.1173675	2.075777848 ±0.0445717	2.121479459 ±0.0579635
Fm47	16.62621359 ±4.0171695	16.19642857 ±4.447571	3.911504425 ±0.9501647	4.732142857 ±1.4580138
Fm48	226.4660194 ±70.507888	227.5267857 ±73.686573	382.7876106 ±53.9526	411.6160714 ±45.021966
Fm49	3.429604007 ±0.3250154	3.336771515 ±0.3042898	17.71644832 ±4.985623	17.85810402 ±5.7868268
Fm50	0.320248211 ±0.0171238	0.314629769 ±0.0176282	0.58800234 ±0.0370288	0.585562196 ±0.0544251
Fm51	0.692291916 ±0.0135577	0.692703398 ±0.0109746	0.589307398 ±0.0114986	0.592975664 ±0.0144049
Fm52	0.660506604 ±0.0158015	0.66012208 ±0.0134993	0.564638224 ±0.011288	0.575143985 ±0.0171262
Fm53	0.184840627 ±0.0164084	0.349042779 ±0.0433355	0.107858667 ±0.041445	0.092169757 ±0.0177239
Fm54	0.338311057 ±0.0293208	0.583562218 ±0.0533356	0196811381 ±0.0657056	0.190241046 ±0.0355942
Fm55	2.250447456 ±0.0496852	2.611891532 ±0.1306424	2.127830025 ±0.0570719	2.105883391 ±0.0378132
Fm56	9.169902913 ±1.7517286	17.45535714 ±4.5498013	6.17699115 ±2.3269772	5.776785714 ±1.8778453
Fm57	0.105679352 ±0.0081419	0.177345527 ±0.0177191	0.066287497 ±0.0186986	0.064409315 ±0.0099421
Fm58	0.36756696 ±0.0415076	0.661020643 ±0.0482456	0.26599209 ±0.0755551	0.267419706 ±0.0687715
Fm59	2.277870683 ±0.0824893	3.0217972 ±0.2166343	2.188979329 ±0.0940338	2.150045533 ±0.0755315
Fm60	7.941747573 ±2.1990031	16.48214286 ±4.2637845	5.477876106 ±1.8617261	5.160714286 ±1.5160022
Fm61	143.1165049 ±33.81277	104.1785714 ±38.28137	177.8495575 ±32.195336	192.0357143 ±23.530669
Fm62	5.222186008 ±0.4529834	3.301913767 ±0.410956	9.560688276 ±3.7675137	9.367032142 ±1.6170945
Fm63	0.445978837 ±0.0178515	0.342412596 ±0.0260486	0.541122462 ±0.0663844	0.543209034 ±0.0348325
Fm64	0.641163075 ±0.0093512	0.704676297 ±0.0169457	0.61301216 ±0.0206361	0.609949173 ±0.0167852
Fm65	0.6083242 ±0.0119314	0.667799677 ±0.0205601	0.585401378 ±0.0246681	0.589626801 ±0.02129
Fm66	0.095113686 ±0.0174826	0.465633641 ±0.065198	0.140739937 ±0.0296777	0.1300553 ±0.0457989
Fm67	0.20444006 ±0.0322448	0.704132305 ±0.0718495	0.264384456 ±0.0576325	0.25348562 ±0.0724192
Fm68	2.140701799 ±0.0780316	3.167516866 ±0.2901199	2.220750894 ±0.1055337	2.191745588 ±0.0859168
Fm69	4.90776699 ±1.3920463	27.875 ±8.7003417	6.637168142 ±2.2522288	5.785714286 ±1.8030433
Fm70	0.07835088 ±0.0103173	0.254631103 ±0.0330093	0.097870439 ±0.0185557	0.094275174 ±0.0230338
Fm71	0.17394733 ±0.0710342	0.824790393 ±0.0520848	0.359691863 ±0.0750951	0.362715902 ±0.0938198
Fm72	2.152677124 ±0.1233912	3.360195018 ±0.5122966	2.248515746 ±0.1078008	2.285049616 ±0.1543873
Fm73	3.849514563 ±1.1735603	20.36607143 ±8.8337962	5.274336283 ±1.4531234	5.678571429 ±2.0099495
Fm74	82.66990291 ±15.381895	41.69642857 ±17.929712	75.87610619 ±18.548745	84.34821429 ±16.674796
Fm75	8.504728751 ±1.2171565	2.740199709 ±0.3100864	6.560479636 ±1.1570252	7.282852796 ±2.057254
Fm76	0.604712135 ±0.0283418	0.355954728 ±0.0282872	0.549893892 ±0.0362535	0.564059837 ±0.0544364
Fm77	0.60817234 ±0.02439	0.749523766 ±0.0249155	0.625933412 ±0.0226299	0.620765878 ±0.0303663
Fm78	0.553211386 ±0.0249427	0.70428249 ±0.031026	0.579084714 ±0.0249868	0.580270964 ±0.0333864
Fm79	0.135454432 ±0.030183	0.951142857 ±0.0498449	0.462453897 ±0.1325108	0.375410138 ±0.0585507
Fm80	0.334796488 ±0.043707	0.994314939 ±0.0092843	0.711532114 ±0.1113483	0.653142825 ±0.0745373

Feature	Normal	Ball defect	Inner race defect	Outer race defect
Fm81	2.395378191 ±0.0959423	22.99165289 ±10.881495	3.375090551 ±0.4578594	3.090771221 ±0.3634527
Fm82	8.344660194 ±2.413912	115.1160714 ±9.6532173	25.63716814 ±12.925654	17.30357143 ±4.3719814
Fm83	0.122120408 ±0.014123	0.655745155 ±0.1066729	0.269069408 ±0.0519422	0.241278521 ±0.0359541
Fm84	0.196569287 ±0.0999731	0.992741121 ±0.0092815	0.701251716 ±0.1680758	0.653211119 ±0.0751844
Fm85	2.201996134 ±0.147097	24.00804997 ±10.79096	3.22885909 ±0.5767167	3.108048965 ±0.4402066
Fm86	4.854368932 ±2.1680958	118.5 ±10.718343	20.5840708 ±8.7471686	17.41071429 ±6.6840587
Fm87	76.72330097 ±16.736294	4.071428571 ±3.8548303	43.82300885 ±20.646787	62.76785714 ±20.980034
Fm88	6.350313909 ±1.1680335	1.102056144 ±0.1059226	2.400102266 ±0.7969911	2.837111991 ±0.401633
Fm89	0.534890639 ±0.0359785	0.060150978 ±0.0391398	0.305773543 ±0.0709794	0.358037012 ±0.0356796
Fm90	0.631422287 ±0.0201355	0.966376114 ±0.0235105	0.75449229 ±0.047507	0.730428761 ±0.0240787
Fm91	0.578492714 ±0.0252204	0.95705336 ±0.0260362	0.720323853 ±0.0567627	0.699909592 ±0.0337998

	Best features obtained by error plot
	Best features obtained by feature selection algorithms

Table 1 (F1 to F13) are the features likely represent a subset of the total features derived, focusing on a specific set of characteristics or metrics that were initially selected or deemed significant for fault diagnosis while Table 2 (Fm1 to Fm91), represents the complete set of features derived from the DWT and RQA process, offering a comprehensive view of the signal's behavior across various frequency bands and patterns.

Classification Using All 91 Features: The dataset containing 91 features was partitioned into training and testing sets in a 70:30 ratio and passed through various classifiers. Here the training accuracy refers to the percentage of correct predictions made by a model on the data it was trained on. It indicates how well the model has learned the patterns from the training data. Testing accuracy refers to the percentage of correct predictions made by the model on new, unseen data (the test set). It measures how well the model generalizes to new data and indicates its performance in real-world scenarios. Remarkably, all classifiers achieved 100% accuracy. Table 3 displays the training and testing accuracies obtained from each classifier. Additionally, the scatter plot of Recurrence Rate and Determinism illustrates the prediction rate of the trained model, demonstrating a 100% prediction accuracy across all four class predictions, as evidenced in Table 3. Furthermore, Fig. 6 shows the confusion matrix for the trained models of all the classifiers, which signifies that the classifier has classified all the observations in each of its true classes correctly. In the confusion matrix Labels are denoted as 1, 2, 3 and 4 for Normal data, Ball Fault, Inner Race and Outer Race respectively.

Table 3. Accuracy for training and testing with 91 features

Models	Accuracy	
	Training	Testing
Linear Discriminant	100%	100%
Quadratic SVM	100%	100%
Cubic SVM	100%	100%

Classification Using 2 Best Features: Feature F15 and F18 were identified as the best features through error bar analysis for feature selection, as illustrated in Fig. 7. In this analysis, the dataset containing only features F15 and F18 was partitioned into training and testing sets in a 70:30 ratio and passed through all classifiers. Table 4 summarizes the training and testing accuracies obtained from all classifiers. Additionally, Fig. 8 illustrates the confusion matrices for QSVM, CSVM, and LDA. These matrices reveal certain misclassifications: the Linear Discriminant classifier misclassified 19 ball defects and 11 inner race defects as outer race defects, 15 outer race defects as ball defects, and 18 outer race defects as inner

Table 4. Accuracy for training and testing with feature 15 and 18

Models	Accuracy	
	Training	Testing
Patternnet	84.3%	85.2%
Linear Discriminant	83.5%	80.2%
Quadratic SVM	83.2%	86.4%
Cubic SVM	82.7%	85.7%

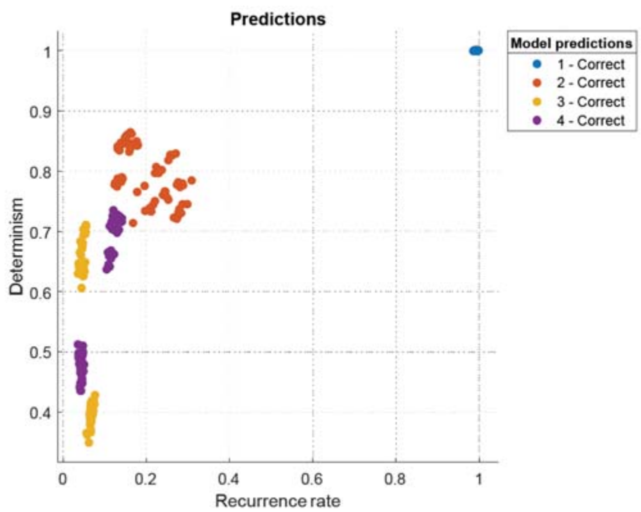

Fig. 5: Scatter plot for features 1 and 2

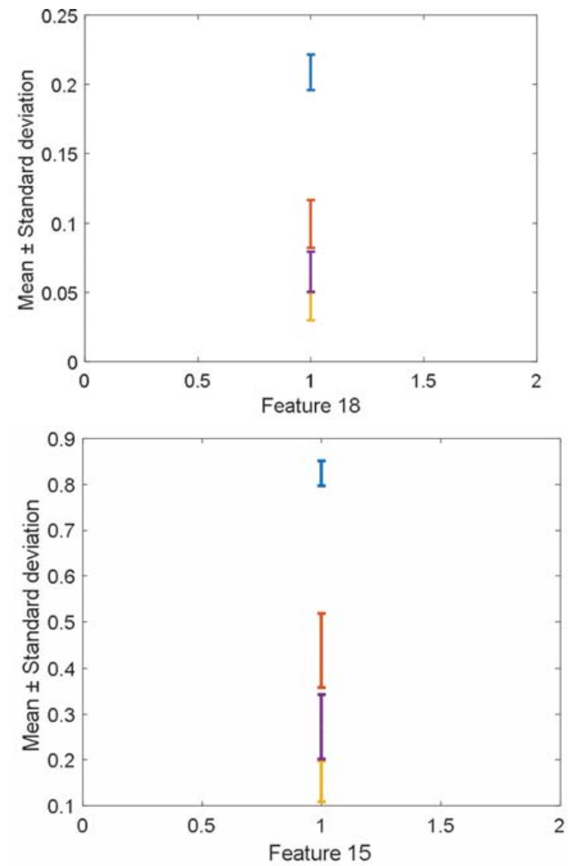

Fig. 7: Error bar for (a) feature 15 (Overlapping defects) and (b) feature 18 (Non Overlapping Defects)

race defects. The Quadratic SVM classifier misclassified 21 ball defects and 24 inner race defects as outer race defects, 12 outer race defects as ball defects, and 7 outer race defects as inner race defects. Lastly, the Cubic SVM classifier misclassified 26 ball defects and 26 inner race defects as outer race defects, 7 outer race defects as ball defects, and 7 outer race defects as inner race defects.

Classification Using Different Feature Selection Algorithms (FSA): In this method, Features were selected using feature selection algorithms like MRMR, Chi-squared, Relief Features, ANOVA, and Kruskal Wallis algorithms. The following features were selected as the best and were common among all the FSA – Fm23, Fm84, Fm9, Fm63, Fm79, Fm10, Fm5, Fm1, Fm82, Fm89, Fm88, Fm2, Fm22, Fm62, Fm11, Fm54, Fm57, Fm64, Fm80, Fm87, Fm83.

Here, the data with these 21 features were divided into testing and training sets in the ratio 70:30 passed through all the classifiers. Table 5 shows the training and testing accuracies obtained from all the classifiers. Fig. 9 shows the

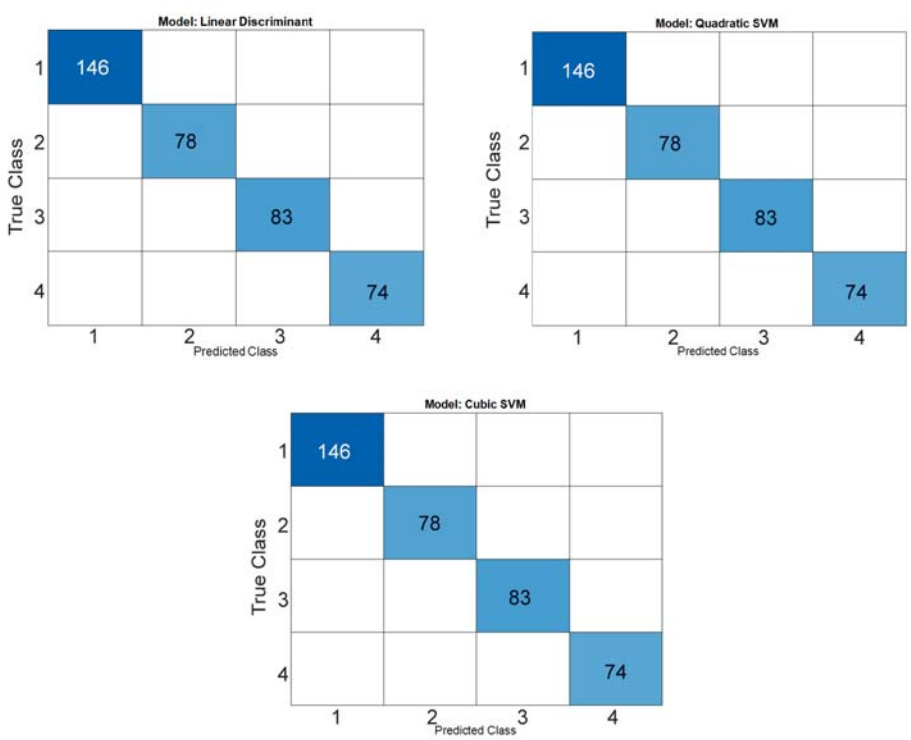

Fig. 6: Confusion matrix for Linear discriminant Analysis, Quadratic SVM and Cubic SVM with 91 features

confusion matrix for QSVM, CSVM and LDA, which signifies that the Linear discriminant classifier has classified 6 outer race defects as inner race defects, the Quadratic SVM classifier has classified 1 inner race defect as outer race defects and cubic SVM has classified 1 inner race defect as outer race defect.

Conclusions

In conclusion, this study utilized a comprehensive approach to motor bearing fault diagnosis through vibration data analysis. Advanced techniques, including Discrete Wavelet Transform (DWT) and feature selection methods, were employed to effectively detect and classify bearing faults. Initially, an analysis of 91 features extracted from DWT coefficients yielded perfect training and testing accuracy. Subsequently, two optimal features, F15 and F18, were identified using error plots, leading to promising classification results across various models, with training accuracies ranging from 82.7% to 84.3% and testing accuracies between 80.2% and 86.4%. The Quadratic Support Vector Machine (QSVM) demonstrated the highest testing accuracy, underscoring its effectiveness in fault diagnosis. Further evaluation using feature selection algorithms showed that the Linear Discriminant classifier achieved 98.4% training accuracy and 98.8% testing accuracy, while both the Quadratic SVM and Cubic SVM reached 99.7% training accuracy, with the Quadratic SVM also attaining 98.8% testing accuracy and the

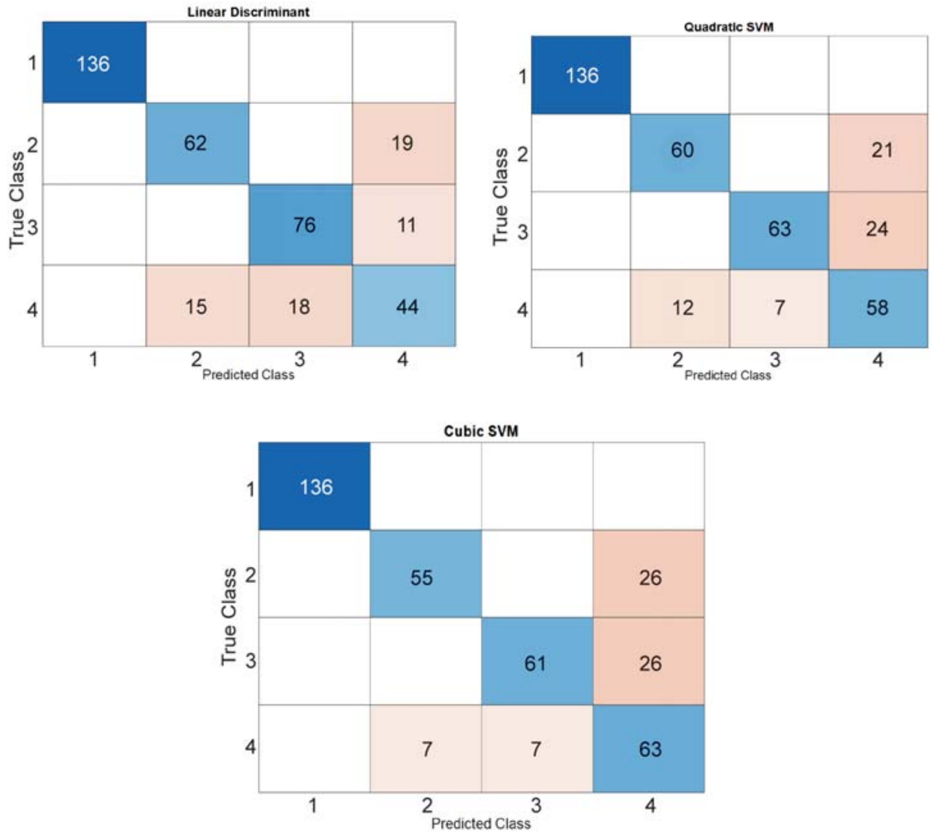

Fig. 8: Confusion matrix for linear discriminant, quadratic SVM and cubic SVM with features 15 and 18

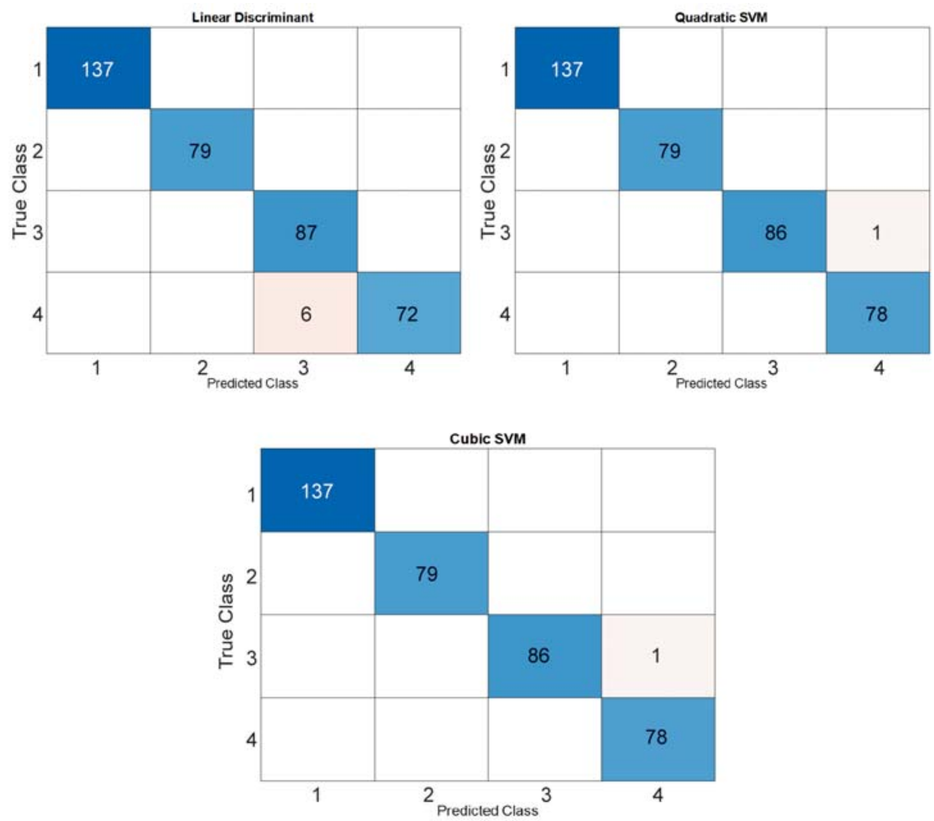

Fig. 9: Confusion matrix for linear discriminant, quadratic SVM, and cubic SVM with selected features

Table 5. Accuracy for training and testing with selected features

Models	Accuracy	
	Training	Testing
Linear Discriminant	98.4%	98.8%
Quadratic SVM	99.7%	98.8%
Cubic SVM	99.7%	100%

Cubic SVM achieving a perfect 100% testing accuracy.

The study demonstrates that feature selection combined with advanced classifiers significantly enhances fault diagnosis accuracy in motor bearings. The QSVM and Cubic SVM, in particular, stand out for their high performance, with the Cubic SVM achieving perfect testing accuracy, indicating its superior capability for precise fault classification. Additionally, comparing the two feature selection methodologies revealed that feature selection algorithms outperformed error plots in identifying the most effective features for classification. ❒

References

1. TAI Commission, Final Report, Rail Inquiry 07-114: Derailment Caused by a Wheel Bearing Failure, Huntly on 19 October 2007, available at: https://www.taic.org.nz/sites/default/files/inquiry/documents/07-114 Final.pdf.
2. S. Airport, Main Landing Gear Wheel Failure Involving a Boeing 737, ZK-ZQB, (2014), available at: https://www.atsb.gov.au/media/5304677/AO-2014-109 Final.pdf.
3. B. Ambrozkiewicz, N. Meier, Y. Guo, G. Litak, and A. Georgiadis, *IOP Conf. Ser.: Mater. Sci. Eng.* **710**, 012014 (2019).
4. D.-F. Wang, Y. Guo, X. Wu, J. Na, and G. Litak, *Appl. Sci.* **10**, 932 (2020).
5. R. N. Toma, Y. Gao, and J.-M. Kim instead of R. Nishat Toma and J.-M. Yangde Gao, *Front. Artif. Intell. Appl.* **364**, 64 (2022).
6. Y. Hsueh, V. R. Ittangihala, W.-B. Wu, H.-C. Chang, and C.-C. Kuo, *Energies* **12**, 3221 (2019).
7. Y. Zhou, R. Zhu, H. Zhao, and X. Zuo, *Measurement* **205**, 112158 (2022).
8. F. Ferracuti, A. Freddi, S. Longhi, and A. Monteriu, in *IEEE Industrial Electronics Society*, 3691-3696 (2019).
9. T. H. Mohamad, Y. Chen, Z. Chaudhry, and C. Nataraj, *J. Softw. Eng. Appl*. **11**, 181 (2018).
10. D. Xiao, Y. Huang, C. Qin, H. Shi, and Y. Li, *Shock Vib*. **2019**, 8325218 (2019).
11. S. Hou, L. Li, R. Bo, W. Wang, and T. Wang, *IEEE*, 43–46, (2011).
12. Y. Qian, R. Yan, and S. Hu, *IEEE Trans. Instrum. Meas*. 63, 2599 (2014).
13. N. Marwan, J. F. Donges, Y. Zou, R. V. Donner, and J. Kurths, *Phys. Lett. A* **373**, 4246 (2009).
14. A. Sharma, AI driven data fusion techniques for health assessment of rotary systems, Ph. D. Thesis, Engineering Sciences (CSIR-NAL), AcSIR, 2024.